

An Analysis of the Latest Super Geomagnetic Storm of the 23RD Solar Cycle (May 15, 2005, Dst : -247 nT)

F. Basciftci*

Vocational School of Technical Sciences, Map and Cadastre Program, Karamanoglu Mehmetbey University, Karaman, Turkey

*e-mail: ffanbasciftci@gmail.com

Received May 10, 2021; revised June 30, 2021; accepted September 24, 2021

Abstract—A geomagnetic storm is a major disturbance in the Earth’s magnetosphere due to the solar wind entering the magnetosphere and ionosphere, lasting about 1–3 days. Storms are known by different categorical names such as weak, moderate, strong (intense), severe (very intense). This study aims to make a mathematical analysis of the latest super geomagnetic storm of the 23rd solar cycle (Dst : -247 nT) which occurred on May 15, 2005. The variables of the study are solar wind parameters (Bz , E , P , N , v , and T) and zonal geomagnetic indices (Dst , ap , and AE). The value range and deviations of variables were defined by the descriptive analysis and the binary relationships of the data were shown by the covariance matrix. A factor analysis was carried out with the help of normal distributions of data and the event (geomagnetic storm) was discussed with linear and nonlinear models. Finally, nonlinear model is also created with solar wind pressure (P), proton density (N), and the ap index. This model explains the storm with an accuracy of 87.5%. In general, this study aims to help the reader understand the storm by presenting models in which parameters and inscription coexist.

DOI: 10.1134/S0016793222010029

1. INTRODUCTION

Geomagnetic storms are well-known features of space weather and usually occur as a result of the transfer of energy from the Solar Wind (SW) to the Magnetosphere of the Earth through magnetic reconnections under various solar events (Reddybattula et al., 2019). Space weather affects the magnetosphere-ionosphere—thermosphere systems and causes geomagnetic/ionospheric storms. During a solar flare or coronal mass ejection (CME), space weather is greatly affected by the speed and intensity of the solar wind and the interplanetary magnetic field carried by the solar wind plasma (de Abreu et al., 2017; Şentürk, 2020).

Adverse space weather conditions affect the accuracy and reliability of communication and satellite systems such as Global Navigation Satellite System (GNSS), Wide Area Augmentation System (WAAS), Very Low Frequency (VLF)/High Frequency (HF)/Ultra-High Frequency (UHF), leading to range errors in satellite signals, rapid phase and amplitude fluctuations (Şentürk, 2020). Recently, there has been an increasing interest in studies examining the behavior of space weather during geomagnetic storms, recently (Fejer et al., 2017; Zhang et al., 2017; Eroglu, 2018, 2019; Klimenko et al., 2018; Okoh et al., 2018; Sharma et al., 2018; Qian et al., 2019; Zhang et al., 2019; Inyurt, 2020a; Koklu, 2020; Piersanti et al., 2020).

Geomagnetic storms consisting of three stages: sudden commencement, main phase, and recovery are some of the most important actions involving dynamic structures (Akasofu, 1964; Burton et al., 1975; Eroglu, 2020; Koklu, 2020). The storm reaction of the dynamic structure begins with CME. CME causes changes in solar wind parameters, leading to the degradation of ionospheric electric fields at medium and low latitudes (Inyurt, 2020a). However, it is not known exactly how CME interacts with the ejection speed and the southward orientation of the magnetic field to affect the electric field and cause a geomagnetic storm (Cherniak and Zakharenkova, 2015).

A geomagnetic storm is mainly determined by solar wind plasma parameters (solar wind dynamic pressure (P), electric field (E), magnetic field (Bz), flow speed (v), proton density (N)), and geomagnetic indices (auroral electrojet (AE), planetary index (Kp), disturbance storm time (Dst), equivalent range index (ap)). Geomagnetic indices and solar wind parameters are briefly described below.

The AE index is the horizontal electric currents that form in the polar region ionosphere. The indices expressing these changes in the polar region were first introduced by Davis and Sugiura (1966). These indices are derived from the geomagnetic change in the horizontal component measured in 12 observation stations between latitudes of 61° N to 70° N (Nakamura et al., 2015). 1-minute resolution data from auroral observation stations are extracted from the average

horizontal density value in magnetically the quietest 5 days, and the *AE* index is calculated. The 1-min data obtained from all observation stations are sorted to obtain the largest (*AU*) and the smallest value (*AL*) of these data. The difference between these two values is defined as the *AE* index (*AU-AL*) (Love and Remick, 2007).

The *Kp* index is a geomagnetic storm index that determines the magnetic effects of the planet and is used to study irregular disturbances in the geomagnetic field caused by the sun's rays. It has been continuously produced since 1932. *Kp* index was taken as the weighted average of *K* indices in 13 subauroral observations. The *Kp* index is a quasilogarithmic planetary index obtained from the *ap* index. (De Canck, 2007; Eroglu et al., 2012; Zolesi and Cander, 2014; Inyurt, 2020b). It is derived at 3-hour intervals using earth-based magnetometers worldwide. The *Kp* index takes a value between 0 and 9. It uses a five-level system called the G-scale to indicate the severity of geomagnetic activity, which is both observed and estimated. This scale is used to quickly demonstrate the severity of a geomagnetic storm. This scale varies from G1 to G5. G1 is the lowest level, G5 is the highest level. Conditions below storm level are called G0, but commonly, this value is not used. Each G level has a specific *Kp* value associated with it. G1 scale indicates weak storm for *Kp* index value 5; G2 scale indicates moderate storm for *Kp* index value 6; G3 scale indicates strong storm for *Kp* index value 7; G4 scale indicates severe storm for *Kp* index value 8; G5 scale indicates extreme geomagnetic storm for *Kp* index value 9. (URL-1).

The *ap* index provides an average daily level of geomagnetic activity. Due to the nonlinear relationship of the *K*-scale with magnetometer fluctuations, it does not make sense to average a series of *K*-indices. Instead, each 3-hour *K* value is converted to a linear scale called the *a*-index. The average of 8 *a*-values per day returns the *ap*-index of a given day. For this reason, the *ap*-index is a geomagnetic activity index in which days with high levels of geomagnetic activity have a higher daily *ap*-value (URL-2).

The *Dst* index is an index obtained at 1-hour intervals using low latitude magnetograms from 4 observation stations, showing magnetic storms, degrees, and changes in the ionosphere layer (Mosna et al., 2007; Cahyadi, 2014; Zolesi and Cander, 2014). The index refers to the decrease of the component of the magnetic field in the horizontal plane at the equator. A decrease in *Dst* indicates increased geomagnetic storm intensity. The *Dst* unit is nanoTesla (nT) (Hunsucker and Hargreaves, 2003; Sharma et al., 2010). Geomagnetic storms are classified according to the density of the *Dst* index (Loewe and Prölss, 1997). If the *Dst* index is between -50 and -30 nT this indicates a weak storm. If the *Dst* index is between -100 and -50 nT this indicates a moderate storm. If the *Dst* index is between -200 and -100 nT this indicates a strong

(intense) storm. If the *Dst* index is less than -200, it indicates a severe (very intense) geomagnetic storm.

The interplanetary magnetic field (IMF) is expressed as part of the solar magnetic field, which is carried into space by solar winds. IMF indices (*Bx*, *By*, and *Bz*) are expressed as vector sizes, two components (*Bx* and *By*) of which are parallel to the orbital plane and the third component (*Bz*) of which is perpendicular to the orbital plane. The *Bx* and *By* components are not important for auroral activity. The north-south direction (the *Bz* component) of the interplanetary magnetic field is the most important component for auroral activity (Abraha, 2014; URL-3). The *Bz* component is caused by fluctuations in the solar wind and other effects. When the IMF and geomagnetic field lines are oriented in opposite directions, energy, mass, and momentum transfer from solar wind flow to the magnetosphere occurs (Şentürk, 2018). While the *Bz* component of the magnetic field is in the north direction in calm day conditions, it turns south in the initial phase of the magnetic storm and the storm occurs (Abraha, 2014; Zolesi and Cander, 2014).

The solar wind is a plasma wave emitted from the Sun's upper atmosphere. The solar wind constantly flows out of the Sun and consists mainly of protons and electrons in a condition known as plasma. Different regions of the Sun produce solar wind at different speeds and densities. High-speed winds bring geomagnetic storms, while slow winds bring calm space weather. Determining and predicting solar wind is critical to improving forecasts of space weather and the predictions of its impact on Earth. The solar wind dynamic pressure is a function based on speed and intensity (URL-4). The formula is given below.

$$P = m_p n V^2 = 1.6726 \times 10^{-6} n V^2. \quad (1)$$

In Equation (1), *P* is the pressure in nano Pascal (nPa) unit, *m_p* is the proton mass, *n* is the density in particle/cm³ unit, and *V* is the speed of solar wind in km/h unit (URL-5).

The *E* is a feature of space surrounding the electrical charge or magnetic field and affects the loaded objects in it through electrical power. It is expressed in millivolt/meter (mV/m). An electric field that varies over time (e.g. due to a moving charged particle) causes a local magnetic field. This indicates that the electrical and magnetic fields are not independent of each other (URL-6).

Proton density is used as the measure of activity. The proton density unit is Np/cm³, indicating the number of protons passing through the unit cubic centimeters volume. Proton density increases in slow solar winds, while it decreases in rapid solar winds (Schwenn, 2001). Dashora et al., (2009) showed that the peaks in proton density (>15 proton/cm³) are in direct contact with cases where changes in the *Bz* index, a value of magnetic field index, are over 5 nT (light storm) or below 5 nT (light storm). For this rea-

son, proton density index values greater than 15 protons/cm³ are considered as active space climatic conditions (Ulukavak, 2016).

This study investigated the latest geomagnetic storm of the 23rd solar cycle. The storm took place at level G4 (severe-very intense) ($Dst = -247$ nT) on May 15, 2005. These storms were studied based on solar wind parameters (Bz , E , P , N , v , and T) and geomagnetic indices (Dst , ap , Kp , and AE). The study is organized as follows: In the Data section, the five-day data distributions for the storm (May 13, 2005–May 17, 2005) are presented based on solar parameters and geomagnetic indices. Analysis and explanations are presented in the Mathematical Model section and the discussion in the Conclusion section.

2. DATA

The Interactive Data Language (IDL) based Space Physics Environment Data Analysis Software (SPEDAS) was used in this study. The software can be accessed from the link (URL-7). Hourly OMNI-2 Solar Wind and IMF parameter data are available online. In addition, the AE and Dst indices were obtained from the World Data Center for Geomagnetism Kyoto using the SPEDAS. The Kp and ap indices were taken from National Geophysical Data Center (NGDC) using the SPEDAS with Coordinated Data Analysis (CDA) Web Data Chooser (general data on space physics). Geomagnetic storms are classified according to the intensity of the Dst index. For the Storm of May 15, 2005, the dynamic pressure of solar wind; magnetic field; electric field; flow speed; proton density; temperature, and Dst , ap and AE indices were obtained with the OMNI hourly data.

The geomagnetic storm dated May 15, 2005, at the severe level ($Dst = -247$ nT), which was the latest superstorm of the 23rd solar cycle, was analyzed. Figure 1 shows the OMNI data set from 13 May 2005 0000 UT to 17 May 2005 2359 UT. The chart covers 2 days before the storm, the day of the storm (May 15, 2005) and 2 days after the storm (120 h).

The May storm began with CME on May 15. On May 15, 2005 at 0300 a.m., P suddenly rose to one of its highest values, 24.43 nPa (min: 0.13; max: 30.18 nPa), Bz reached 5.2 nT (min: -36.5 ; max: 21.9 nT), and N rose to its maximum value of 19.2 cm⁻³ (min: 0.3; max: 19.2 cm⁻³). Three hours later, the Bz component fell to -36.5 nT at UT 0600, heading south, AE index reached a maximum of 1184 nT, v increased to 928 km/h. Five hours later, the Kp index and the ap index reached their highest values with 83 nT and 236 nT, respectively, while the Dst index followed them reaching a minimum of -247 nT at 0800 UT.

The components shown in Fig. 1 can be briefly described as follows. On May 15, 2005, at 0600 UT, when the component Bz was at a minimum (-36.5 nT), the Dst index dropped to -58 nT and E reached its highest

value at 33.87 mV/m. In addition, the ap index and the Kp index reached their highest values with 236 nT and 83 nT, respectively, N reached 15.8 cm⁻³, v reached 928 km/h, and the AE index reached a maximum value of 1184 nT. After two hours, the Dst index reached a negative peak value of -247 nT.

On May 15, 2005, 0800 UT when the Dst index showed a minimum value of -247 nT, the Bz component reached -10.4 nT, E 9.52 mV/m, the ap index 236 nT, the Kp index 83 nT, v 915 km/h, N 6.0 cm⁻³, P 12.82 nPa and AE index 933 nT.

On May 15, 2005, 1000 AM UT, when the Bz component reached a maximum (21.9 nT), E the lowest value of -20.63 mV/m, N 2.5 cm⁻³, P 4.15 nPa, v 942 km/h, the ap index 179 nT, the Kp index 77 nT, and the AE index 409 nT. As a result, the Dst index was -184 nT.

3. MATHEMATICAL MODEL

Pearson's correlation analysis, given in Table 1 for the May 2005 geomagnetic storm, is a parametric statistical method that shows the direction, degree, and importance of the relationship between the variables. The relationship is strengthened when the value between the two variables approaches ± 1 (Eroglu, 2019; Inyurt, 2020a). Physically, in this storm, $Bz-E$, $T-N-P$, $N-P$, $v-P-Kp-Dst-ap$, $P-ap$ groups have a strong correlation.

KMO (Kaiser-Meyer-Olkin) and Bartlett Test help to understand the suitability of variables for factor analysis. The KMO test value close to 1.0 indicates that the data is suitable for factor analysis. KMO values between 0.8 and 1.0 indicate that sampling is in good condition. KMO values below 0.6 indicate that sampling is not sufficient and corrective action is required. Some researchers accept this value at 0.5, so a judgment can be used for values between 0.5 and 0.6. In this study, the Kaiser-Meyer-Olkin Measure of Sampling Adequacy was found to be 0.64. With this value obtained, the variables of this storm are suitable for factor analysis.

Kaiser normalization and basic component analysis are appropriate analyses for subgrouping data. Variables divided into subgroups show maximum eigenvalues with the highest contribution approach. The change in the storm can be modeled with three maximum eigenvalues at 87% (Table 2).

The Varimax Rotation Matrix method indicates the linear clustering of variables. In this method, where each variable is treated as a factor along with the weight values, the event is discussed through linear models as a whole. According to the Rotated component matrix, linear models of variables can be written in two components. The values of the variables according to the 1st component; Obtained as $Bz -0.020$, $T 0.077$, $N 0.064$, $v 0.828$, $P 0.314$, $E -0.003$, $Kp 0.869$, $Dst 0.865$, $ap 0.837$ and $AE 0.632$. The values of the

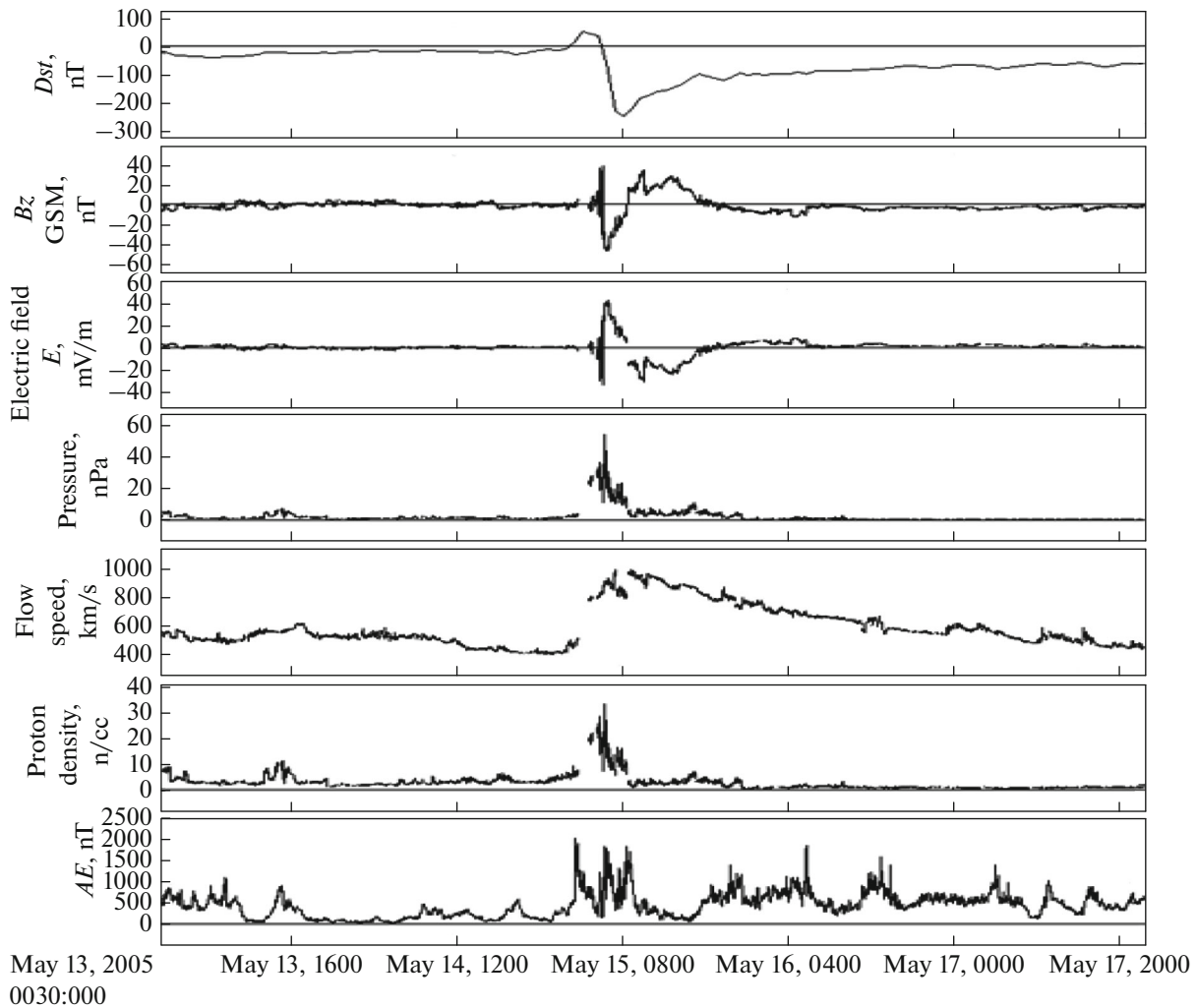


Fig. 1. Top to bottom: Dst index (nT), B_z magnetic field (nT), electric field (E ; mV/m), solar wind dynamic pressure (P ; nPa), flow speed (v ; km/h) and proton density (N ; cm^{-3}) and aurora electrojet (AE ; nT) index are shown for May 13–15, 2005 (from NASA's NSSDC OMNI data set).

variables according to the 1st component; Obtained as $B_z -0.014$, $T 0.917$, $N 0.977$, $v 0.318$, $P 0.908$, $E 0.062$, $Kp 0.280$, $Dst 0.346$, $ap 0.318$ and $AE 0.099$. The linear models resulting from the weights of the data presented above can be written as follows.

$$\text{Axes 1} = -0.020B_z + 0.077T + 0.064N + 0.828v + 0.314P - 0.003E + 0.869Kp - 0.865Dst + 0.837ap + 0.632AE;$$

$$\text{Axes 2} = -0.014B_z + 0.917T + 0.977N + 0.318v + 0.908P + 0.062E + 0.280Kp + 0.346Dst + 0.318ap + 0.099AE.$$

Figures 2a–2c shows the physical distribution of the Dst , ap and AE geomagnetic indices by solar wind parameters, respectively. According to Figs. 2a–2c, the physical reaction of zonal geomagnetic indices to the change in solar wind parameters during the storm process can be summarized as follows. While Dst 's reaction T , N , and v is linear, its reaction B_z , P , and E

is not linear. While ap index's reaction N and v is linear, its reaction B_z , T , P , and E is not linear. While AE index's reaction B_z , N and v is linear, its reaction T , P , and E is not linear.

Linear models of Dst , ap , and AE indices are produced by solar wind parameters. According to the independent variables (solar wind parameters), linear compounds of the dependent variables Dst , ap and AE are given in Table 3. According to Table 3, linear models of Dst , ap , and AE indexes are given below, respectively.

$$Dst = 106.321 + 1.187B_z + 9.630N - 0.318v, \text{ the multiple determination coefficient, here, is } R 0.908.$$

$$ap = -104.017 - 2.637B_z + 2.062 \times 10^{-5}T + (0.224)v, \text{ the multiple determination coefficient, here, is } R 0.785.$$

$$AE = -192.011 - 145.603B_z + 0.946v - 140.395E, \text{ the multiple determination coefficient, here, is } R 0.758.$$

Table 1. The Pearson's correlation matrix for storm variables

	<i>Bz</i>	<i>T</i>	<i>N</i>	<i>v</i>	<i>P</i>	<i>E</i>	<i>Kp</i>	<i>Dst</i>	<i>ap</i>	<i>AE</i>
<i>Bz</i>	1	-0.072	-0.034	0.246**	-0.072	-0.992**	-0.122	-0.092	-0.226*	-0.435**
<i>T</i>		1	0.844**	0.316**	0.798**	0.113	0.311**	0.217*	0.379**	0.171
<i>N</i>			1	0.353**	0.921**	0.075	0.340**	0.297**	0.355**	0.168
<i>v</i>				1	0.576**	-0.236**	0.705**	-0.684**	0.665**	0.358**
<i>P</i>					1	0.114	0.475**	0.012	0.534**	0.281**
<i>E</i>						1	0.107	0.120	0.231*	0.387**
<i>Kp</i>							1	-0.539**	0.867**	0.653**
<i>Dst</i>								1	-0.582**	-0.363**
<i>ap</i>									1	0.525**
<i>AE</i>										1

* Correlation is significant at the 0.05 level (2-tailed). ** Correlation is significant at the 0.01 level (2-tailed).

Table 2. Total variance explained

Component	Initial eigenvalues			Rotation sums of squared loadings		
	total	% of variance	cumulative %	total	% of variance	cumulative %
1	4.262	42.621	42.621	3.399	33.989	33.989
2	2.320	23.199	65.820	3.036	30.358	64.347
3	2.204	22.044	87.864	2.352	23.518	87.864

Table 3. Regression coefficients for geomagnetic indices *Dst*, *ap* and *AE*

Geomagnetic Indexes	Model	Unstandardized coefficients		Standardized coefficients	t	Sig.
		B	Std. Error	Beta		
<i>Dst</i>	(Constant)	106.321	8.504		12.502	0.000
	<i>Bz</i> (nT)	1.187	0.294	0.164	4.040	0.000
	<i>N</i> (cm ⁻³)	9.630	0.635	0.638	15.173	0.000
	<i>v</i> (km/h)	-0.318	0.015	-0.949	-21.892	0.000
<i>ap</i>	(Constant)	-104.017	11.644		-8.933	0.000
	<i>Bz</i> (nT)	-2.637	0.401	-0.395	-6.572	0.000
	<i>T</i> (K)	2.062E-005	0.000	0.122	1.985	0.050
	<i>v</i> (km/h)	0.224	0.020	0.724	11.448	0.000
<i>AE</i>	(Constant)	-192.011	71.225		-2.696	0.008
	<i>Bz</i> (nT)	-145.603	19.262	-3.740	-7.559	0.000
	<i>v</i> (km/h)	0.946	0.113	0.525	8.370	0.050
	<i>E</i> (mV/m)	-140.395	21.646	-3.201	-6.486	0.000

As seen in Pearson's correlation matrix for storm variables in Table 1, there is a strong correlation between the *Dst* and *ap* indices and *v*. The relationship between *Dst* and *ap* indices and *v* can be seen in Fig. 3. Table 4 show the analysis values between *Dst* and *ap* to *v*, respectively. Table 4 shows that the model between *Dst* and *ap* and *v* is significant. Also, according to Table 4, the linear model between flow speed (*v*) and

Dst and the linear model between flow speed (*v*) and *ap* are shown below, respectively.

$Dst = 76.309 - 0.229v$, where the correlation coefficient *R* is 0.684. $ap = -88.473 + 0.216v$, where the correlation coefficient *R* is 0.665.

Although plasma flow speed is seen as a control mechanism for dynamic pressure (Burton et al., 1975),

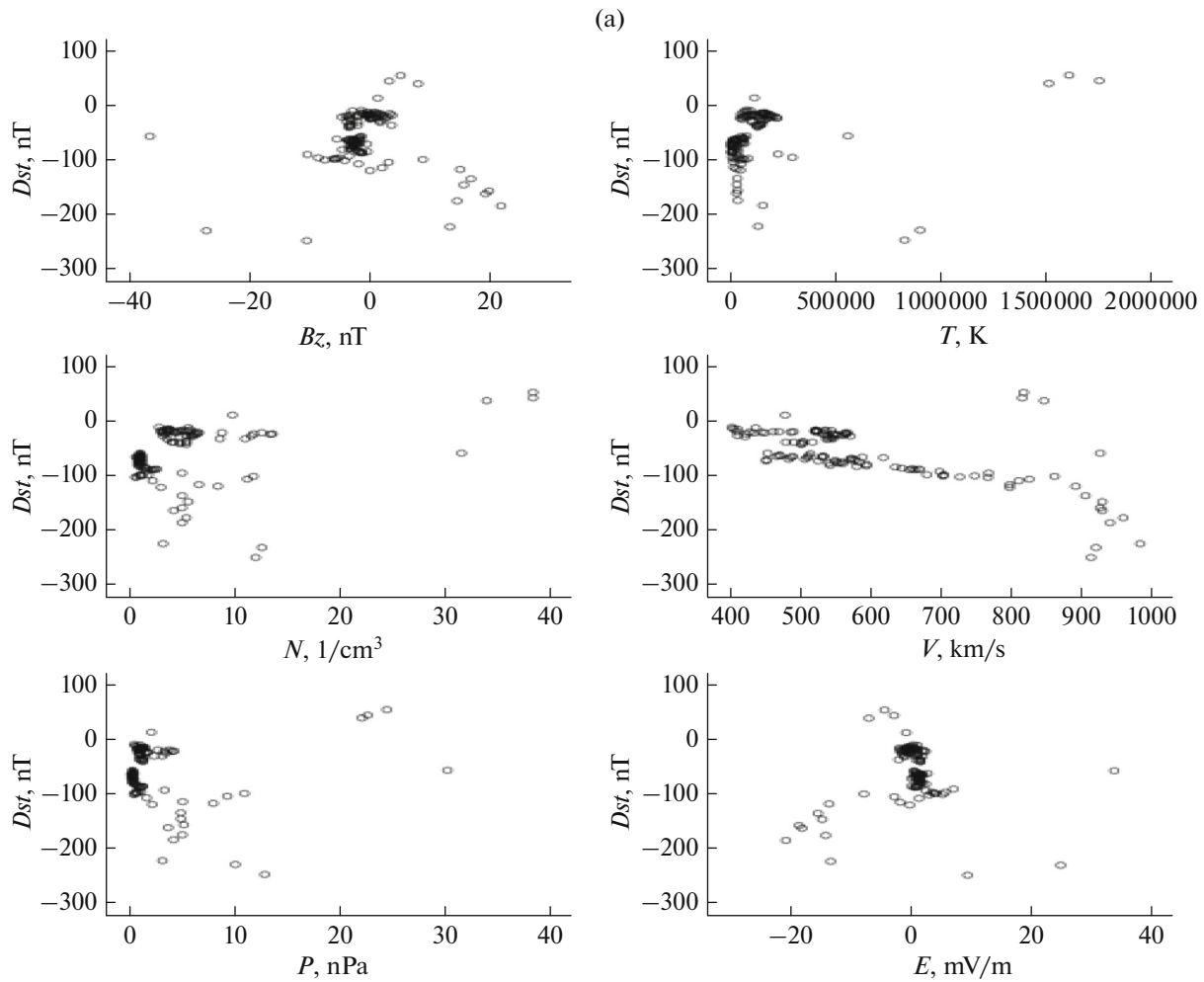


Fig. 2. (a) The appearance between *Dst* index and the solar wind parameters *Bz*, *T*, *N*, *v*, *P*, *E*. (b) The appearance between *ap* index and the solar wind parameters *Bz*, *T*, *N*, *v*, *P*, *E*. (c) The appearance between *AE* index and the solar wind parameters *Bz*, *T*, *N*, *v*, *P*, *E*.

magnetic field and proton density are also a necessary predictive tool of the *Dst* index. Physically, coronal holes created by hot electron fluctuation and radiation are the source of high-speed solar wind currents

(Tsurutani et al., 2006; Adhikari et al., 2019). Nonlinear fluctuations in the high-speed solar wind and negative reductions in *Bz* (peaks) are vital for geomagnetic activity. The flow speed and nonlinear motion in the

Table 4. Analysis of Variance and Regression coefficient for *Dst* and *ap* geomagnetic indices

Geomagnetic indexes	Model	Sum of squares	df	Mean square	F	Model	Unstandardized coefficients		Standardized coefficients	t	Sig.
							B	Standard error	Beta		
<i>Dst</i>	Regression	137893.735	1	137893.735	103.553	(Constant)	76.309	13.858	-0.684	5.507	0.000
	Residual	157131.590	118	1331.624		<i>v</i> (km/s)	-0.229	0.023		-10.176	0.000
	Total	295025.325	119								
<i>ap</i>	Regression	110928.154	1	110928.154	93.505	(Constant)	-88.473	13.080	0.665	-6.764	0.000
	Residual	139987.046	118	1186.331		<i>v</i> (km/s)	0.206	0.021		9.670	0.000
	Total	250915.200	119								

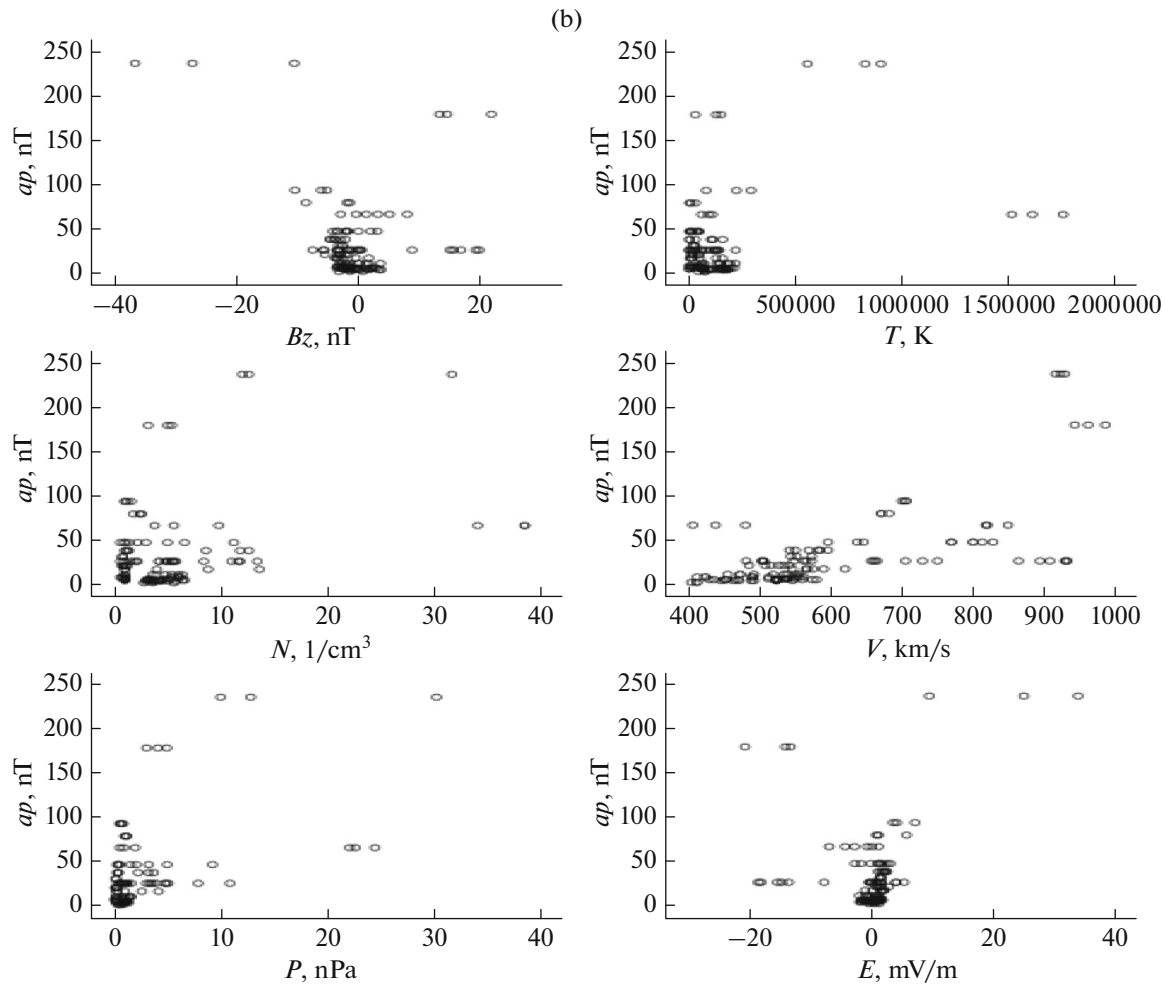


Fig. 2. (Contd.).

B_z component indicate that it is time for the Dst index to peak. At the onset of a geomagnetic storm, the density of protons increases, which affects the magnetosphere. High-density plasma pressure with low speed compresses the magnetosphere (Tsurutani et al., 2006). This means that the storm begins for the magnetosphere-ionosphere, driven by the solar wind (Borovsky and Yakymenko, 2017). Since this compression and disturbance is shown by the Dst index, the researchers try to increase the Dst forecast values with connection functions shaped by solar wind parameters, where the speed parameter (Borovsky, 2012) cannot be selected (Gonzalez et al., 1987; 1989).

The high-density plasma pressure that compresses the magnetosphere can be discussed in the same model as the ap index (Eroglu, 2018, 2019; Inyurt, 2020a). The proven model consists of dynamic pressure, proton density, and ap index. Physically, dynamic pressure (P) and proton density (N) are linearly affected by fluctuations in the magnetic field, while the reaction of the ap index to these fluctuations is logarithmic. The model including P , N , and ap is

presented in Table 5. The nonlinear model is $P = a + b \ln(ap) + cN$; where a , b , c is fixed. Table 5 shows that with the analysis of variance values, all parameter estimates are in the 95% confidence interval. In addition, according to Table 5, the coefficients of the model are $a = -3.043$, $b = 0.782$ and $c = 1.248$. The model explaining this storm with an accuracy of 87.5%

$$P = -(3.043) + (0.782)\ln ap + (1.248)N.$$

4. CONCLUSIONS

This study focused on the super geomagnetic storm on May 15, 2005, with a Dst index value of -247 nT. Since this is the latest superstorm of the 23rd solar cycle, it was meticulously analyzed based on solar wind parameters and zonal geomagnetic indices. The boundaries of the variables were determined with the descriptive analysis, the binary relationships between the variables with the correlation matrix. In addition, the relationship between zonal geomagnetic indices and solar wind parameters and their interactions with each other are illustrated with graphs and tables. The

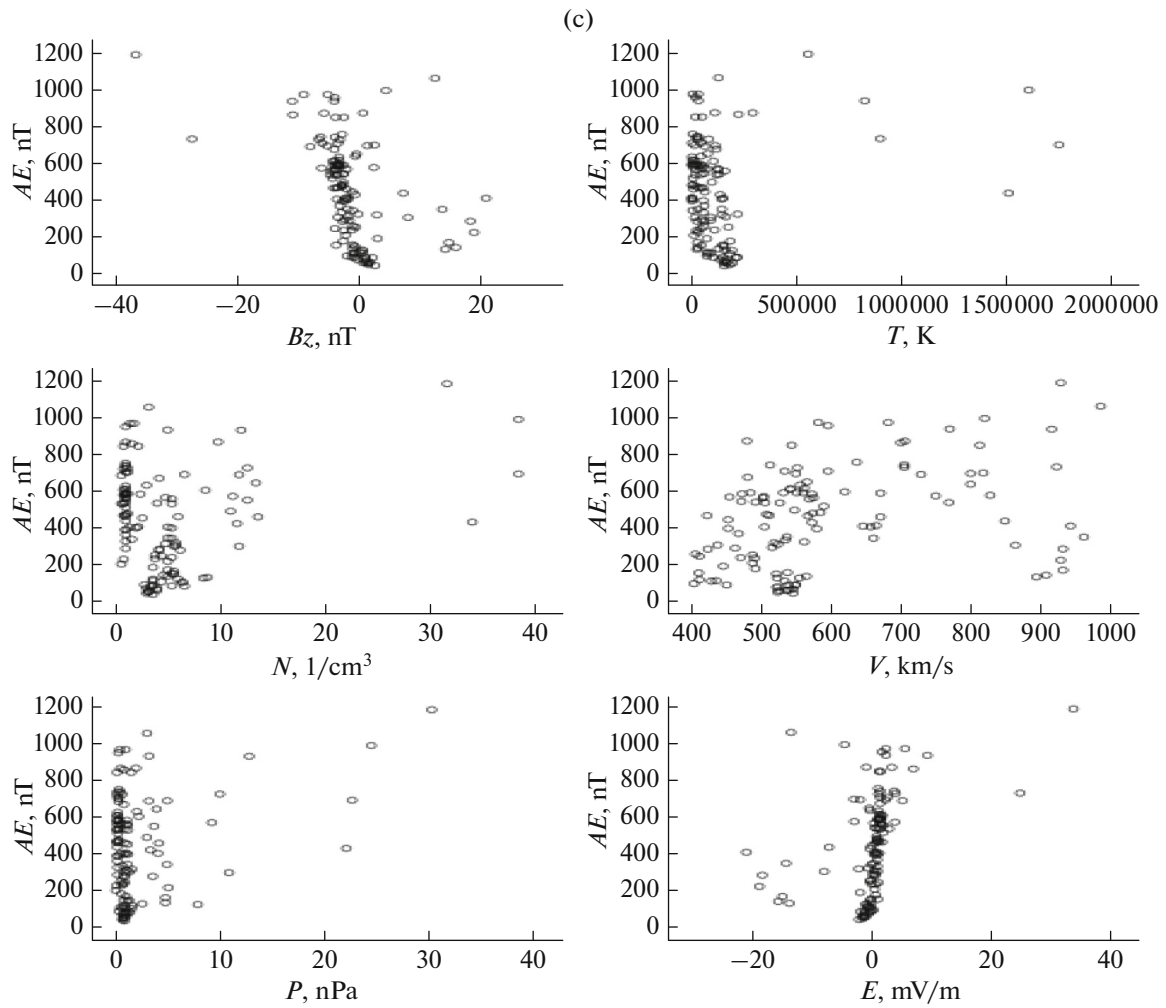


Fig. 2. (Contd.).

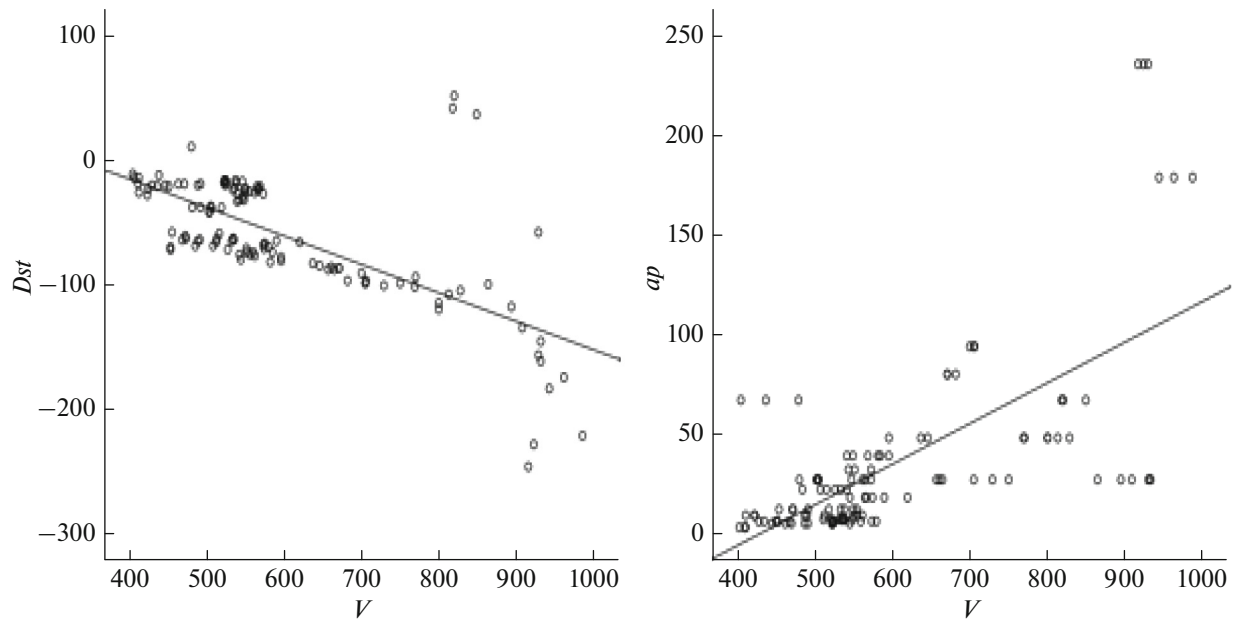


Fig. 3. The linear relationship between Dst and ap indices and flow speed (v).

Table 5. ANOVA (Analysis of Variance) and Parameter Estimates of the model including P , N , and ap

Source	Sum of squares	df	Mean Squares	Parameter	Estimate	Standard error	95% Confidence interval	
							Lower bound	Upper bound
Regression	3038.883	3	1012.961	a	-3.043	0.467	-3.968	-2.118
Residual	335.816	117	2.870	b	0.782	0.157	0.470	1.093
Uncorrected Total	3374.699	120		c	1.248	0.050	1.149	1.346
Corrected Total	2693.113	119						

data were analyzed mathematically and the models were created. Finally, the study was completed with a nonlinear model between solar wind dynamic pressure (P), proton density (N), and ap index. The modeling of the geomagnetic storm on May 15, 2005, was successful at a rate of 87.5%. The model that coincides with the studies in the literature expresses itself with high accuracy. Moreover, all results are within the confidence interval of 95%. In future studies, the author plans to analyze other storms of the 23rd solar cycle.

ACKNOWLEDGMENTS

I thank the NASA CDA Web for OMNI Database (<http://themis.igpp.ucla.edu/software.shtml>), Kyoto (University) World Data Center, and National Geophysical Data Center.

REFERENCES

- Abraha, G., Total electron content (TEC) variability of low latitude ionosphere and role of dynamical coupling: Quiet and storm-time characteristics, *PhD Thesis*, Addis Ababa University, Ethiopia, 2014.
- Adhikari, B., Adhikari, N., Aryal, B., Chapagain, N.P., and Horvath, I., Impacts on proton fluxes observed during different interplanetary conditions, *Sol. Phys.*, 2019, vol. 294, no. 5.
<https://doi.org/10.1007/s11207-019-1450-6>
- Akasofu, S.I., The development of the auroral substorm, *Planet Space Sci.*, 1964, vol. 12, no. 4, pp. 273–282.
- Borovsky, J.E., The velocity and magnetic field fluctuations of the solar wind at 1 AU: Statistical analysis of Fourier spectra and correlations with plasma properties, *J. Geophys. Res.: Space Phys.*, 2012, vol. 117, no. A5, A05104.
<https://doi.org/10.1029/2011JA017499>
- Borovsky, J.E. and Yakymenko, K., Systems science of the magnetosphere: Creating indices of substorm activity, of the substorm-injected electron population, and of the electron radiation belt, *J. Geophys. Res.: Space Phys.*, 2017, vol. 122, no. 10, pp. 10012–10035.
<https://doi.org/10.1002/2017JA024250>
- Burton, R.K., McPherron, R.L., and Russell, C.T., An empirical relationship between interplanetary conditions and *Dst*, *J. Geophys. Res.*, 1975, vol. 80, no. 31, pp. 4204–4214.
<https://doi.org/10.1029/JA080i031p04204>
- Cahyadi, M.N., Near-field coseismic ionospheric disturbances of earthquakes in and around Indonesia, *PhD Thesis*, Hokkaido University Collection of Scholarly and Academic Papers, 2014.
- Cherniak, I. and Zakharenkova, I., Dependence of the high-latitude plasma irregularities on the auroral activity indices: A case study of 17 March 2015 geomagnetic storm, *Earth Planets Space*, 2015, vol. 67, no. 1, id 151.
<https://doi.org/10.1186/s40623-015-0316-x>
- Dashora, N., Sharma, S., and Dabas, R., S., Alex, S., and Pandey, R., Large enhancements in low-latitude total electron content during 15 May 2005 geomagnetic storm in Indian zone, *Ann. Geophys.*, 2009, vol. 27, no. 5, pp. 1803–1820.
<https://doi.org/10.5194/angeo-27-1803-2009>
- Davis, T.N. and Sugiura, M., Auroral electrojet activity index *AE* and its universal time variations, *J. Geophys. Res.*, 1966, vol. 71, no. 3, pp. 785–801.
<https://doi.org/10.1029/JZ071i003p00785>
- De Abreu, A.J., Martin, I.M., Fagundes, P.R., Venkatesh, K., Batista, I.S., de Jesus, R., Rockenback, M., Coster, A.J., Gende, M., Alves, M.A., and Wild, M., Ionospheric *F*-region observations over American sector during an intense space weather event using multi-instruments, *J. Atmos. Sol.-Terr. Phys.*, 2017, vol. 156, pp. 1–14.
<https://doi.org/10.1016/j.jastp.2017.02.009>
- De Canck, M.H., Ionosphere properties and behaviors, *Antennex*, 2007, vol. 119, pp. 6–7.
- Eroglu, E., Aksoy, S., Tretyakov, O.A., Surplus of energy for time-domain waveguide modes, *Energy Educ. Sci. Technol.*, 2012, vol. 29, no. 1, pp. 495–506.
- Eroglu, E., Mathematical modeling of the moderate storm on 28 February 2008, *New Astron.*, 2018, vol. 60, pp. 33–41.
<https://doi.org/10.1016/j.newast.2017.10.002>
- Eroglu, E., Modeling the superstorm in the 24th solar cycle, *Earth Planets Space*, 2019, vol. 71, id 26.
<https://doi.org/10.1186/s40623-019-1002-1>
- Eroglu, E., Modeling of 21 July 2017 geomagnetic storm, *J. Eng. Technol. Appl. Sci.*, 2020, vol. 5, no. 1, pp. 33–49.
<https://doi.org/10.30931/jetas.680416>
- Fejer, B.G., Blanc, M., and Richmond, A.D., Post-storm middle and low-latitude ionospheric electric fields effects, *Space Sci. Rev.*, 2017, vol. 206, nos. 1–4, pp. 407–429.
<https://doi.org/10.1007/s11214-016-0320-x>

- Gonzalez, W.D. and Tsurutani, B.T., Criteria of interplanetary parameters causing intense magnetic storms ($Dst < -100$ nT), *Planet Space Sci.*, 1987, vol. 35, no. 9, pp. 1101–1109.
[https://doi.org/10.1016/0032-0633\(87\)90015-8](https://doi.org/10.1016/0032-0633(87)90015-8)
- Gonzalez, W.D., Tsurutani, B.T., Gonzalez, A.L.C., Smith, E.J., Tang, F., and Akasofu, S.I., Solar wind–magnetosphere coupling during intense magnetic storms (1978–1979), *J. Geophys. Res.*, 1989, vol. 94, no. A7, pp. 8835–8851.
<https://doi.org/10.1029/JA094iA07p08835>
- Hunsucker, R.D. and Hargreaves, J.K., *The High-Latitude Ionosphere and Its Effects on Radio Propagation*, Cambridge: Cambridge University Press, 2003.
- Inyurt, S., Modeling and comparison of two geomagnetic storms, *Adv. Space Res.*, 2020a, vol. 65, no. 3, pp. 966–977.
<https://doi.org/10.1016/j.asr.2019.11.004>
- Inyurt, S., Investigation of ionospheric variations during magnetic storm over Turkey, *Geomagn. Aeron.*, 2020b, vol. 60, no. 1, pp. 131–135.
<https://doi.org/10.1134/S0016793220010120>
- Klimenko, M.V., Klimenko, V.V., Despirak, I.V., Zakharenkova, I.E., Kozelov, B.V., Cherniakov, S.M., Andreeva, E.S., Tereshchenko, E.D., Vesnin, A.M., Korenkova, N.A., Gomonov, A.D., Vasiliev, E.B., and Rатовsky, K.G., Disturbances of the thermosphere–ionosphere–plasmasphere system and auroral electrojet at 30° E longitude during the St. Patrick's Day geomagnetic storm on 17–23 March 2015, *J. Atmos. Sol.-Terr. Phys.*, 2018, vol. 180, pp. 78–92.
<https://doi.org/10.1016/j.jastp.2017.12.017>
- Koklu, K., Mathematical analysis of the 09 March 2012 intense storm, *Adv. Space Res.*, 2020, vol. 66, no. 4, pp. 932–941.
<https://doi.org/10.1016/j.asr.2020.04.053>
- Loewe, C.A. and Pröls, G.W., Classification and mean behavior of magnetic storms, *J. Geophys. Res.*, 1997, vol. 102, no. A7, pp. 14209–14213.
<https://doi.org/10.1029/96JA04020>
- Love, J.J. and Remick, K.J., Magnetic indices, in *Encyclopedia of Geomagnetism and Paleomagnetism*, Springer, 2007, pp. 509–512.
- Mošna, Z., Šauli, P., and Santolík, O., Preparation of a database for the study of scaling phenomena in the ionosphere, in *WDS'07 Proceeding of Contributed Papers*, 2007, vol. 2, pp. 86–92.
- Nakamura, M., Yoneda, A., Oda, M., and Tsubouchi, K., Statistical analysis of extreme auroral electrojet indices, *Earth Planets Space*, 2015, vol. 67, no. 1, id 153.
<https://doi.org/10.1186/s40623-015-0321-0>
- Okoh, D., Onwuneme, S., Seemala, G., Jin, S., Rabi, B., Nava, B., and Uwamahoro, J., Assessment of the NeQuick-2 and IRI-Plas 2017 models using global and long-term GNSS measurements, *J. Atmos. Sol.-Terr. Phys.*, 2018, vol. 170, pp. 1–10.
<https://doi.org/10.1016/j.jastp.2018.02.006>
- Piersanti, M., De Michelis, P., Del Moro, D., Tozzi, R., Pezzopane, M., Consolini, G., Marcucci, M.F., Laurenza, M., Di Matteo, S., Pignalberi, A., Quattrociochi, V., and Diego, P., From the Sun to the Earth: August 25, 2018 geomagnetic storm effects, *Ann. Geophys.*, 2020, vol. 38, pp. 703–724.
<https://doi.org/10.5194/angeo-2019-165>
- Qian, L., Wang, W., Burns, A.G., Chamberlin, P.C., Coster, A., Zhang, S.R., and Solomon, S.C., Solar flare and geomagnetic storm effects on the thermosphere and ionosphere during 6–11 September 2017, *J. Geophys. Res.: Space Phys.*, 2019, vol. 124, no. 3, pp. 2298–2311.
<https://doi.org/10.1029/2018JA026175>
- Reddybattula, K.D., Panda, S.K., Ansari, K., and Peddi, V.S.R., Analysis of ionospheric TEC from GPS, GIM and global ionosphere models during moderate, strong, and extreme geomagnetic storms over Indian region, *Acta Astronaut.*, 2019, vol. 161, pp. 283–292.
<https://doi.org/10.1016/j.actaastro.2019.05.042>
- Schwenn, R., Solar wind: Global properties, in *Encyclopedia of Astronomy and Astrophysics*, Bristol: Institute of Physics, 2001.
- Sharma, K., Dabas, R.S., and Sarkar, S.K., Das, R.M., Ravindran, S., and Gwal, A.K., Anomalous enhancement of ionospheric F2 layer critical frequency and total electron content over low latitudes before three recent major earthquakes in China, *J. Geophys. Res.*, 2010, vol. 115, no. A11, pp. 4–9.
<https://doi.org/10.1029/2009JA014842>
- Sharma, S.K., Ansari, K., and Panda, S.K., Analysis of ionospheric TEC variation over Manama, Bahrain, and comparison with IRI-2012 and IRI-2016 models, *Arab. J. Sci. Eng.*, 2018, vol. 43, pp. 3823–3830.
<https://doi.org/10.1007/s13369-018-3128-z>
- Şentürk, E., Temporal, spatial, spectral and statistical investigation of seismic–ionospheric precursors of Turkey earthquakes using GPS/GNSS measurements, *PhD Thesis*, Kocaeli: Kocaeli University, 2018.
- Şentürk, E., Investigation of global ionospheric response of the severe geomagnetic storm on June 22–23, 2015 by GNSS-based TEC observations, *Astrophys. Space Sci.*, 2020, vol. 365, id 110.
<https://doi.org/10.1007/s10509-020-03828-z>
- Tsurutani, B.T., Gonzalez, W.D., Gonzalez, A.L.C., Guarneri, F.L., Gopalswamy, N., Grande, M., Kamide, Y., Kasahara, Y., Lu, G., Mann, I., McPherron, R., Soraas, F., and Vasyliunas, V., Corotating solar wind streams and recurrent geomagnetic activity: A review, *J. Geophys. Res.: Space Phys.*, 2006, vol. 111, no. A7.
<https://doi.org/10.1029/2005JA011273>
- Ulukavak, M., Investigation of The Relationship Between Equatorial and Mid-Latitude Earthquakes with Ionospheric TEC Anomalies, *PhD. Thesis*, Karadeniz Technical University, Trabzon (in Turkish), 2016.
- URL-1. The Kp-index. <https://www.spaceweatherlive.com/en/help/the-kp-index.html>. Accessed January 23, 2021.
- URL-2. The Ap-index. <https://www.spaceweatherlive.com/en/help/the-ap-index.html>. Accessed January 23, 2021.
- URL-3. The Interplanetary Magnetic Field (IMF). <https://www.spaceweatherlive.com/en/help/the-interplanetary-magnetic-field-imf.html>. Accessed January 23, 2021.
- URL-4. Solar Wind. <https://www.swpc.noaa.gov/phenomena/solar-wind>. Accessed February 06, 2021.
- URL-5. Solar Wind. https://en.wikipedia.org/wiki/Solar_wind#cite_note-38. Accessed: February 06, 2021.

- URL-6.* Electric field. https://tr.wikipedia.org/wiki/Elektrik_alan%C4%B1. Accessed February 06, 2021.
- URL-7.* Space Physics Environment Data Analysis Software. <http://themis.igpp.ucla.edu/software.shtml>, Accessed: February 06, 2021.
- Zhang, R. and Liu, L., Le, H., Chen, Y., Equatorial ionospheric electrodynamics over Jicamarca during the 6–11 September 2017 space weather event, *J. Geophys. Res.: Space Phys.*, 2019, vol. 124, no. 2, pp. 1292–1306. <https://doi.org/10.1029/2018JA026295>
- Zhang, S.R., Zhang, Y., Wang, W., and Verkhoglyadova, O.P., Geospace system responses to the St. Patrick’s Day storms in 2013 and 2015, *J. Geophys. Res.: Space Phys.*, 2017, vol. 122, no. 6, pp. 6901–6906. <https://doi.org/10.1002/2017JA024232>
- Zolesi, B. and Cander, L.R., *Ionospheric Prediction and Forecasting*, Berlin: Springer, 2014.